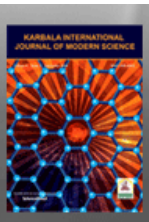

Karbala International Journal of Modern Science

Volume 8 | Issue 3 Article 16

Continuum Damping Effects in Nuclear Collisions

Hossein Sadeghi
Department of Physics, Faculty of Science, University of Arak, Arak 8349-8-38156, Iran, H-Sadeghi@araku.ac.ir

Mahdieh Ghafouri
Department of Physics, Faculty of Science, University of Arak, Arak 8349-8-38156, Iran

Recommended Citation

Sadeghi, Hossein and Ghafouri, Mahdieh (2022) "Continuum Damping Effects in Nuclear Collisions," *Karbala International Journal of Modern Science*: Vol. 8 : Iss. 3 , Article 16.
Available at: https://doi.org/10.33640/2405-609X.3238

Continuum Damping Effects in Nuclear Collisions

Abstract

The Time-Dependent Skyrme Hartree-Fock (TDSHF) calculations have been conducted to study 100Sn+16O, 116Sn+16O, and 122Sn+16O collisions on a 3-Dimensional (3D) mesh with SV-bas SF. For the 100Sn+16O collision, the continuum damping width of the rotational amplitudes in Ecm = 100, 150, 200, and 250 MeV has been achieved around 108, 185, 277, and 318, with the time evolution width for z2 around 15/5, 13/5, 13/9, or 14/3 fm2. The quadrupole deformation, kinetic energy, and rotational amplitude are studied. It is seen that the compound nucleus becomes uniform and spherical as time grows. The results of the time evolution show the continuum damping effects after the fusion phase. The damping mechanism is related to removing the dependence on the size of the box. The results were compared with the available experimental and theoretical results.

Keywords

Time-Dependent Skyrme Hartree-Fock; Heavy-Ion Collisions; Quadrupole Deformation; Damping Effects

RESEARCH PAPER

Continuum Damping Effects in Nuclear Collisions

Mahdieh Ghafouri, Hossein Sadeghi*

Department of Physics, Faculty of Science, University of Arak, Arak, 8349-8-38156, Iran

Abstract

The Time-Dependent Skyrme Hartree-Fock (TDSHF) calculations have been conducted to study $^{100}Sn+^{16}O$, $^{116}Sn+^{16}O$, and $^{122}Sn+^{16}O$ collisions on a 3-Dimensional (3D) mesh with SV-bas SF. For the $^{100}Sn+^{16}O$ collision, the continuum damping width of the rotational amplitudes in $E_{cm} = 100$, 150, 200, and 250 MeV has been achieved around 108, 185, 277, and 318, with the time evolution width for z^2 around 15/5, 13/5, 13/9, or 14/3 fm^2. The quadrupole deformation, kinetic energy, and rotational amplitude are studied. It is seen that the compound nucleus becomes uniform and spherical as time grows. The results of the time evolution show the continuum damping effects after the fusion phase. The damping mechanism is related to removing the dependence on the size of the box. The results were compared with the available experimental and theoretical results.

Keywords: Time-dependent skyrme Hartree-Fock, Heavy-ion collisions, Quadrupole deformation, Damping effects

1. Introduction

Understanding the isotopic properties of different nuclei is the most interesting and important subject in the field of nuclear physics. One of the projects in this field in recent years has been the investigation of the static nuclei properties. Knowing the energy spectra of the different isotopes of nuclei is one such subject. Since various scattering experiments have shown that nucleons move with kinetic energy (10 MeV) inside the nuclei, this energy is compared to the inertial energy of nucleons, which is around (1000 MeV). Whatever the relativistic effects of the nucleon's motion, we can use non-relativistic quantum mechanics to study the energy spectrum of nuclei. The Time-dependent Density Function Theory (TDFT) is a Time-Dependent Hartree-Fock (TDHF) that has been quite effective in the study of nuclear dynamics [1−9]. The effective interaction of Skyrme Force (SF) with many of its parameters during runtime, using the static and TDFT methods, enables microscopic computation of low-energy heavy-ion collisions. For nuclear collisions with higher excited energies, TDHF without pairing is an acceptable approximation. The calculations are usually carried out in 3D Cartesian space under Periodic Boundary Conditions (PBC) [10,11]. Over time and with increasing computing power, TDHF calculations became possible using precise numerical calculations [12−19]. The theory of TDHF can be analyzed according to the principle of change, which is expressed as time-dependent.

The Sky3D code in the coordinate space is used for TDHF calculations based on the Skyrme energy function. Sky3D code solves static or dynamic equations in 3D Cartesian space [20]. The spinors of the nucleon wave functions are displayed on a 3D Cartesian mesh without additional symmetric constraints. The code resolves TDHF equations with an extension of the time operator [10]. In recent decades, with the increase in computational capacity, large-scale TDHF calculations have also become possible [21,22].

Recently we calculated the binding energy, and charge radius, using the Skyrme-Hartree-Fock-Bogolyubov (SHFB) method and the density-dependent pairing interaction [23]. The results show the existence of a regular statistical behavior for all investigated stable nuclei. In addition, this behavior becomes more consistent with the

Received 24 February 2022; revised 18 May 2022; accepted 23 May 2022.
Available online 1 August 2022

* Corresponding author.
E-mail address: H-Sadeghi@araku.ac.ir (H. Sadeghi).

https://doi.org/10.33640/2405-609X.3238

increase in the mass of the selected nuclei. On the other hand, the average magnitude of quadrupole deformation in heavy nuclei is higher than in other mass ranges and there is a direct relationship between the magnitude of the deformation and the regular behavior. This can be accounted combination of rotational and vibrational modes of motion and hence the order of the structure of these nuclei increases. The current study's goal is to investigate the effect of neutron to proton ratio in the structure of these nuclei, the effect of spin, the deformation of the structure of nuclei, and so on.

The work is structured as follows: In Section 2, we briefly present the theoretical framework to describe how to obtain the different observables that we presented in the work. The results of the binding energies, the kinetic energy, the quadrupole deformation, and the continuum damping effects persisting after the fusion phase are given in section 3. Section 4 summarizes the results.

2. A brief review of the theoretical framework

A nucleus in the ground state single-particle (*s.p*) wave functions is expressed as follows [23,24].

$$\left(\frac{-\hbar^2}{2m}\nabla^2 + V(\rho\{\psi\})\right)\psi_\alpha(\vec{r}) = \varepsilon_\alpha\psi_\alpha(\vec{r}) \tag{1}$$

where ε_α is the s.p energy for the 'α' position leads to a static solution with the following phase factor

$$\exp^{i\overrightarrow{k}.\vec{r}}\psi_\alpha\left(\overrightarrow{r} - \frac{\hbar\overrightarrow{k}}{m}t\right) \tag{2}$$

For the net density dependence, we need to add expressions that include vibrational and rotational modes to the density function. In static calculations, some constraints can be used to solve many situations for solving static TDHF equations. The most common of these is the constraint used in quadrupole, using the expectation value [24].

$$\widehat{H} \to \widehat{H} - \lambda\left(2z^2 - x^2 - y^2\right) \tag{3}$$

The TDHF equations can be analyzed in Slater determinant wave function space [5] or obtained with TDHF, depending on how both the system modes and the desired observations are optimized.

The static wave functions are displayed as $\psi_{\alpha,\,I}^{state}\,t$ that I = 1 and 2, which stands for the two nuclei. The collisions must have a larger numerical box than the static Hartree-Fock calculations. For nuclear reactions, the Slater state is the starting configuration with *s.p* wave functions that are shifting and amplified, see Ref. [10].

An analysis of the TDHF equations is given in Refs. [25,26], beginning with the time-dependent Schrödinger equation,

$$i\hbar\frac{\partial}{\partial t}|\psi_\alpha(t)\rangle = \widehat{H}|\psi_\alpha(t)\rangle \tag{4}$$

where interacting Hamiltonian may be defined as

$$\begin{aligned}\widehat{H} &= \widehat{T} + \widehat{V} = \sum_{\alpha\beta} t_{\alpha\beta}a_\alpha^+ a_\beta \\ &+ \frac{1}{2}\sum_{\alpha\beta\gamma\delta} V_{\alpha\beta\gamma\delta}a_\alpha^+ a_\beta^+ a_\gamma a_\delta\end{aligned} \tag{5}$$

where $t_{\alpha\beta}$ and $V_{\alpha\beta\gamma\delta}$ are kinetic energy and two-body interaction matrix elements, respectively. The a_i^+ operator creates a particle in state i and the a operator destroys a particle in state i.

The TDHF equations are obtained as follows, see Ref. [10]:

$$S = \int \mathrm{dt}\left[E[\{\psi_\alpha\}] - \sum_\alpha \langle\psi_\alpha|i\partial_t|\psi_\alpha\rangle\right] \tag{6}$$

The energy is given in Eqs. (5a)–(5h) of Ref. [2]. The TDHF equation (Eq. (4)) can be solved in the form of the following integral equation

$$\begin{aligned}|\psi_\alpha(t+\Delta t)\rangle &= U(t,t+\Delta t)|\psi_\alpha(t)\rangle \\ U(t,t+\Delta t) &= \widehat{T}\exp\left(-\frac{i}{h}\int_t^{t+\Delta t}\widehat{H}(t')dt'\right)\end{aligned} \tag{7}$$

where $\hat{T}$ and $\hat{U}$ are the time-ordering and time-evolution operators, respectively.

The energy without considering pairing is given

$$E = E_{\mathrm{kin}} + \int d^3r\left(\varepsilon_{\mathrm{Sk}} + \varepsilon_{\mathrm{Sk}}^{\mathrm{ls}}\right) + E_C \tag{8}$$

where kinetic energy is

$$E_{\mathrm{kin}} = \int d^3r\frac{\hbar^2}{2m}\tau \tag{9}$$

there are some terms derived from the Skyrme force [10].

$$\begin{aligned}\varepsilon_{\mathrm{Sk}} &= \frac{1}{2}b_0\rho^2 + b_1\left(\rho\tau - \vec{J}^2\right) \\ &- \frac{b_2}{2}\rho\Delta\rho + \frac{b_3}{3}\rho^{a+2} - \sum_q\frac{b_0'}{2}\rho_q^2 \\ &+ b_1'\left(\rho_q\tau_q - \vec{J}_q^{\,2}\right) + \frac{b_2'}{2}\rho_q\Delta\rho_q + \frac{b_3'}{2}\rho^a\rho_q^2\Big)\end{aligned} \tag{10}$$

and the spin current

$$\varepsilon_{\mathrm{Sk}}^{(\mathrm{ls})} = -b_4\left[\rho\nabla.\vec{J} + \vec{\sigma}.\left(\nabla\times\vec{J}\right)\right] + b_4'\sum_q\left[\rho_q\nabla.\vec{J}_q + \vec{\sigma}_q.\left(\nabla\times\vec{J}_q\right)\right] \quad (11)$$

The Coulomb energy is given

$$E_C = \frac{e^2}{2}\int d^3\mathrm{r}\mathrm{d}^3r'\rho_p(\vec{r})\frac{1}{|\vec{r}-\vec{r}|}\rho_p(\vec{r}) - \frac{3}{4}e^2\left(\frac{3}{\pi}\right)^{\frac{1}{3}}\int d^3r\left[\rho_p(\vec{r})\right]^{\frac{4}{3}} \quad (12)$$

With

$$\vec{\sigma}_q(\vec{r}) = \sum_q\varphi_\alpha^+(\vec{r})\vec{\sigma}\varphi_\alpha(\vec{r})$$

$$\vec{J}_q(\vec{r}) = -i\sum_q\varphi_\alpha^+(\vec{r})\nabla\times\vec{\sigma}\varphi_\alpha(\vec{r})$$

The 3D SF in both static and TDHF solutions is offered. The grid spacing is usually 1 Fm. The increase in Skyrme energy is shown as [10,23].

$$E_{\mathrm{tot,HF}} = \frac{1}{2}\sum_\alpha((t_\alpha+\varepsilon_\alpha)) + E_{3,\mathrm{corr}} + E_{\mathrm{C,corr}}$$

$$E_{3,\mathrm{corr}} = \int d^3r\frac{\alpha}{6}\rho^\alpha\left[b_3\rho^2 - b_3'\left(\rho_p^2+\rho_n^2\right)\right] \quad (13)$$

$$E_{\mathrm{C,corr}} = \frac{1}{4}\left(\frac{3}{\pi}\right)^{1/3}\int d^3r\rho_{\mathrm{pr}}^{4/3}$$

where ρ is local density and is given

$$\rho_q(r) = \sum_{\alpha\in q}\sum_s v_\alpha^2\left|\psi_\alpha(r,s)\right|^2 \quad (14)$$

That $q = p$ (or n) for protons (or neutrons) and $\rho = \rho_p + \rho_n$ is total density. The coefficients b_3 and b_3' are included in the definition of SF and are described in Ref. [23].

To calculate the total energy, a 3D solver is used (TDSHF) that solves the self-consistent HF equation and the TDHF equations, see Ref. [10] for more details. Numerical computations are performed on a Cartesian 3D grid. All recent SF variations may be properly addressed. For low energies, the Fourier method of Coulomb is a proper solution for isolated charge distribution, nuclear vibrations, and collisions between nuclei. The spherical moments of the quadrupole state are defined as follows

$$Q_{2m}^{(\mathrm{type})} = \int d^3\mathrm{r}\mathrm{r}^2Y_{2m}\rho^{(\mathrm{type})}\left(\vec{r}-\vec{R}\right) \quad (15)$$

where the Cartesian quadrupole is given

$$Q = 2\sin\left(\frac{\pi z}{z_{\mathrm{box}}}\right)^2 - \sin\left(\frac{\pi y}{y_{\mathrm{box}}}\right)^2 - \sin\left(\frac{\pi x}{x_{\mathrm{box}}}\right)^2 \quad (16)$$

There are two shape parameters a_0 and a_2 called deformation β and triaxialityγ which are referred to as Bohr-Mottelson parameters and given

$$\beta = \sqrt{a_0+2a_2^2}, \gamma = \mathrm{atan}\left(\frac{\sqrt{2}a_2}{a_0}\right) \quad (17)$$

More detailed observation energies are supplied by *s.p* energies.

3. Results and discussion

Nuclear collision is a major application of nuclear TDHF equations. This code is designed to make such collision scenarios clearer. 3D TDHF calculations were carried out using the Sky3D code with SV-bas SF for collisions at different energies. This code performs the equations based on Skyrme energy functional and also allows the static version of the equations to determine the ground state structure of nuclei.

Fig. 1(a) and Fig. 1(b) represent the temporal evolution of kinetic energy for frontal collisions relative to collision energies. Greater quadrupole deformation in high collision energies is not associated with greater axial relationships, we see that the volume expansion of compound nuclei plays a role. The final kinetic energies for all four elements are 2108, 2100, 2083, and 2087 MeV. These are smaller than 2134, 2183, 2233, and 2283 MeV the first kinetic energies. These differences explain the conversion of kinetic energies into potential energies. We see that at higher energies for head-to-head collisions, the final kinetic energies are smaller as well as the quadrupole deformation energies are larger.

The boundary condition in the TDSHF collision calculation was performed in 3D coordinate space by examining the collision with the 2 fm collision parameter and finding that the rotation amplitude is also damped.

Table 1 describes the parameters describing Coulomb excitation, which is defined as half the range of the closest approach at 180^o and is the wavelength of de Broglie reduced by the projectile. The values of a and the adiabatic parameter are presented in this table [27].

Fig. 2(a) and Fig. 2(b) show the temporal transformations of the quadrupole deformities resulting from the TDHF calculations of the above collisions.

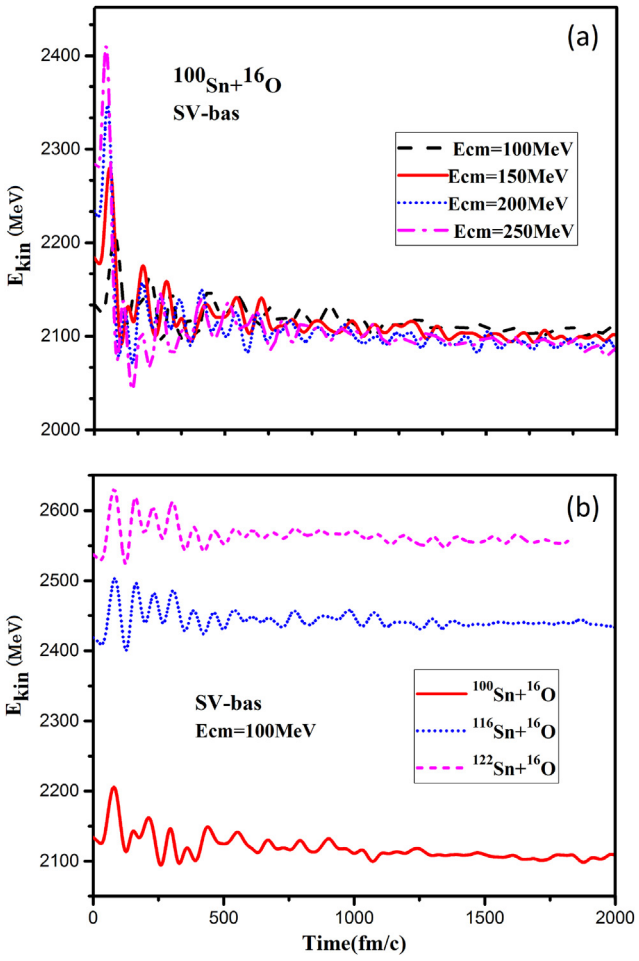

Fig. 1. TDHF results of the kinetic energy time evolution for a) the frontal $^{100}Sn+^{16}O$ collision at different E_{cm} = 100, 150, 200, and b) 250 MeV energies as well as $^{116}Sn+^{16}O$, $^{122}Sn+^{16}O$, and $^{100}Sn+^{16}O$ collisions at E_{cm} = 100 MeV.

In the fusion phase, the oscillations for large amplitudes are strongly damped.

The slopes are larger at higher collision energies. However, the deformation is close to each other in four cases.

The changes in the deformation kinetic energies are not symmetrical. Fusion is not a simple quadrupole deformation damping oscillator because it is density-dependent and exhibits incompressibility. In the equilibrium state, the quadrupole strain is 441, 587, 737, and 858 fm^2, respectively.

To study the rotational evolution, the values of z^2 for different collision energies and the tin isotope collision with ^{16}O with different N/Z ratios are given in Fig. 3(a) and Fig. 3(b). We see how the amplitude of rotation is damped in these results. This damping of rotation is not surprising given the acceptable damping of small-amplitude vibrations. The main goal in the case of vibrations is to compute the excitation spectra by Fourier analyzing the time dependence of relevant observable. The creation of a neck between nuclei, the dissipation of energy from collective motion, processes such as charge transfer, and the approach to fusion are all of the primary interest in collisions. This figure also shows a clear damping image. Vibration damping has been thoroughly studied [28], while the amplitude of rotation damping amplitude has rarely been considered. The temporal evolution results indicate that the continuous damping effect continues after the fusion phase. The continuum damping width of the rotational amplitudes for E$_{cm}$ = 100, 150, 200,

Table 1. Coulomb excitation parameters for Sn.

Projectile	*E*	*a*	*λ*	$\eta = a/\lambda$	€
	MeV	*fm*	*fm*		
^{4}He	10	7.5	0.75	10	0.667
^{16}O	42.0	7.8	0.25	39	0.634

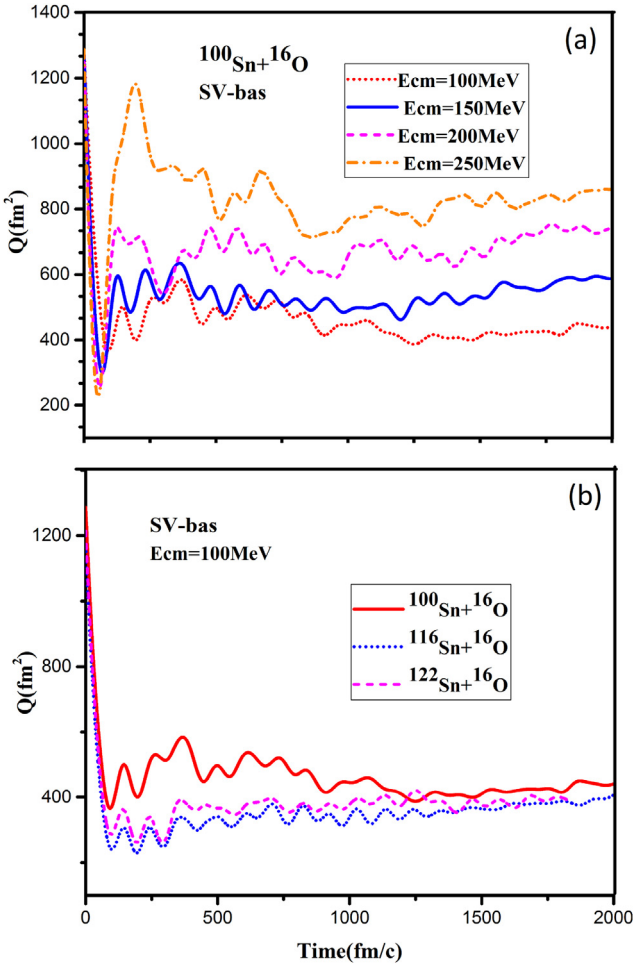

Fig. 2. Calculated quadrupole moments by TDHF for a) the head-to-head $^{100}Sn+^{16}O$ collision at different E_{cm} = 100, 150, 200, and 250 MeV energy as well as b) $^{116}Sn+^{16}O$, $^{122}Sn+^{16}O$, and $^{100}Sn+^{16}O$ collisions at E_{cm} = 100 MeV.

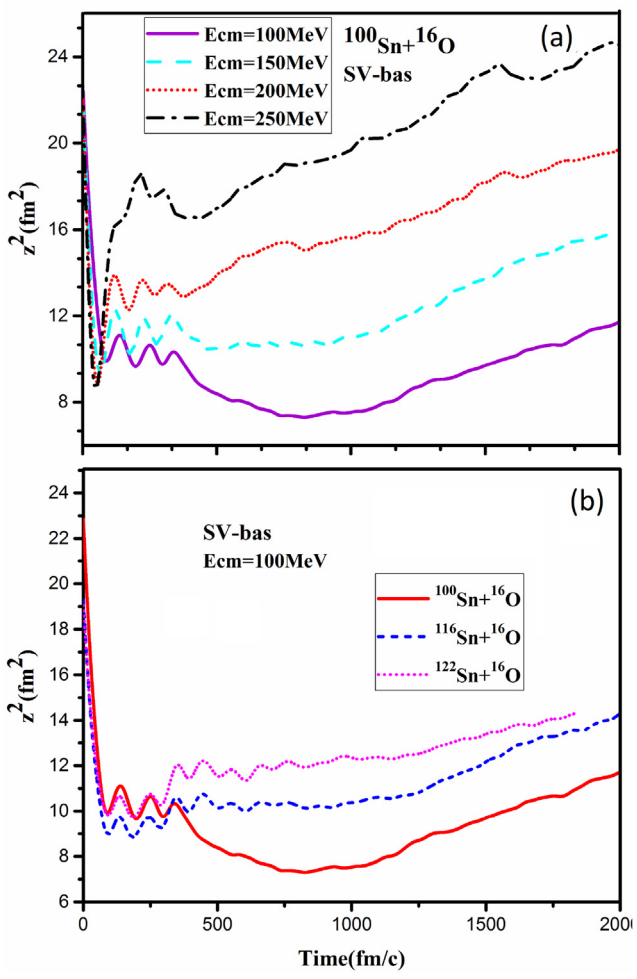

Fig. 3. The results of the time evolution of z^2 for a) the head-to-head $^{100}Sn+^{16}O$ collision at different E_{cm} = 100, 150, 200, and 250 MeV energy as well as b) $^{116}Sn+^{16}O$, $^{122}Sn+^{16}O$, and $^{100}Sn+^{16}O$ collisions at E_{cm} = 100 MeV.

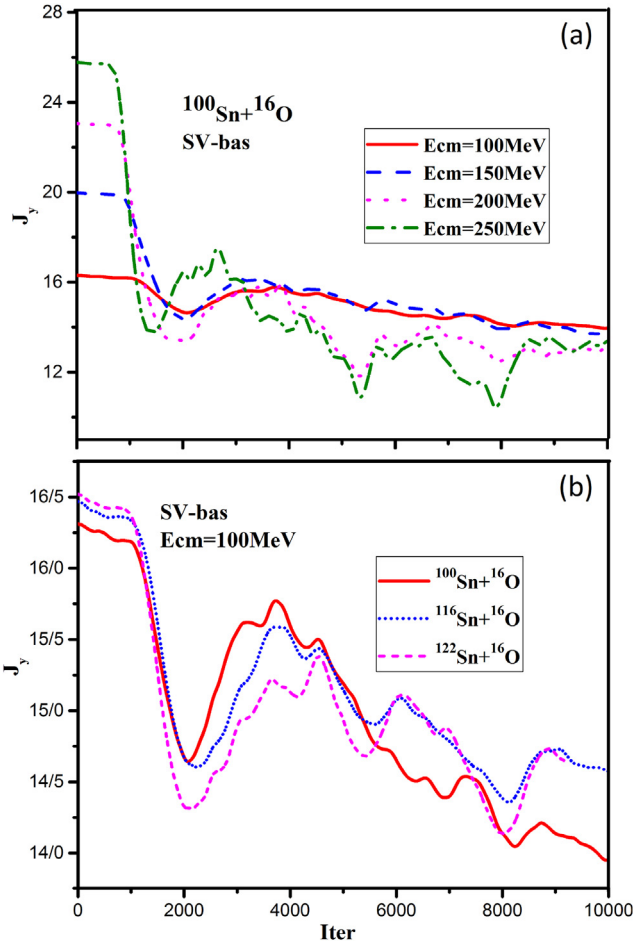

Fig. 4. The result shows the time evolution of the angular momentum Jy for tin isotopes and $^{100}Sn+^{16}O$ a) at different E_{cm} = 100, 150, 200, and 250 MeV energy as well as b) $^{116}Sn+^{16}O$, $^{122}Sn+^{16}O$, and $^{100}Sn+^{16}O$ collisions at E_{cm} = 100 MeV.

and 250 MeV has been achieved around 108, 185, 277, and 318 MeV, with the time evolution width for z^2 around 15.5, 13.5, 13.9, and 14.3 fm^2, respectively.

Fig. 4(a) shows the evolution of angular momentum Jy for $^{100}Sn+^{16}O$ collisions in E_{cm} = 100, 150, 200, and 250 MeV, and Fig. 4(b) also represents the time evolution of angular momentum Jy for $^{100}Sn+^{16}O$, $^{116}Sn+^{16}O$, and $^{122}Sn+^{16}O$ collisions in E_{cm} = 100. For rotation in the *xz*-plane, Jy is calculated to be about 1395, 9631, 3212, and 3975 at 10000 fm/*c* for a ^{100}Sn + ^{16}O collision that decreases smoothly at 100 and 150 MeV, and with more fluctuations observed for 200 and 250 MeV energy. Even if the density distribution is spherical, we find that the angular momentum Jy is not stable, and there is no conservation of total angular momentum.

As shown in Fig. 4(a), higher impact energy gives the larger damping range. For head-to-head collisions in periodic boundary conditions, in lower steps, one observes that the oscillation is somewhat cosine-shaped, but with increasing steps, we see a high damping effect, related to breaking dependence on the size of the box. By examining the collision with the 2 fm impact parameter, we discovered that the rotation amplitude is also dampened. As time increases, we also see a more uniform distribution of surface density, indicating that the compound nucleus has become spherical. As we can see, in stable nuclei due to the presence of more neutrons (N/Z) in their scheme, it is overcome by the Coulomb repulsive force between protons. The results also show a consistent statistical pattern for all stable nuclei. As the mass of the selected nuclei increases, the more coherent behavior increases.

Our goal is to study the properties of stable nuclei in different mass ranges as well as to investigate the influence of different parameters like spin, quadrupole deformation rate, etc. The effect of increasing

(N/Z) the neutron to proton ratio has also been shown. This can overcome the Coulomb repulsion force and provides a good opportunity to study the deformation of nuclei. The results showed a more regular behavior for the investigated stable nuclei with increasing mass of selected nuclei.

4. Summary and conclusion

In this paper, we examine Sky3D code that operates on 3D coordinate spaces. In the $^{100}Sn+^{16}O$ collision with the SV-bas Skyrme force, we see that the damping mechanism refers to removing the dependence on the size of the box. When a collision occurs using the 2 fm collision parameter, we have seen that the amplitude of rotation is also damped. As a result, with increasing energy in frontal collisions, kinetic energies decrease and quadrupole deformations and deformation energies increase. The use of SF brings new effects and amazing problems. This is a new power loss mechanism implied in "spin screw excitation". Problems related to the continued reduction in relative kinetic energy for isolated parts are likely due to boundary interactions. In addition, we see that the density distributions in compound nucleus calculations become spherical. When particles emitted from highly excited compound nuclei, faces the boundary, angular momentum is not protected. The results are consistent with available experimental data and other theoretical work. In heavier nuclei, it is interesting to find out how these effects continue.

Funding

No funding was received to assist with the preparation of this manuscript.

Conflict of interest

Authors state no conflict of interest.

References

[1] A.L. Fetter, J. Dirk Walecka, Quantum theory of many-particle systems, first ed., McGraw-Hill, New York, 1971.
[2] J. Alexander Maruhn, P.-G. Reinhard, E. Suraud, Simple models of many-fermions systems, first ed., Springer-Verlag, Berlin Heiderberg, 2010.
[3] W. John, The mean-field theory of nuclear structure and dynamics, Rev Mod Phys. 54 (1982) 913–1015, https://doi.org/10.1103/RevModPhys.54.913.
[4] T. Nakatsukasa, K. Matsuyanagi, M. Matsuo, K. Yabana, Time-dependent density-functional description of nuclear dynamics, Rev Mod Phys. 88 (2016), 045004, https://doi.org/10.1103/RevModPhys.88.045004.
[5] C. Simenel, Nuclear quantum many-body dynamics – from collective vibrations to heavy-ion collisions, Eur Phys J A. 48 (2012) 152, https://doi.org/10.1140/epja/i2012-12152-0.
[6] S.A. Umar, V.E. Oberacker, Time-dependent HF approach to SHE dynamics, Nucl Phys. 944 (2015) 238–256, https://doi.org/10.1016/j.nuclphysa.2015.02.011.
[7] L. Guo, J. Alexander Maruhn, P.-G. Reinhard, Y. Hashimoto, Conservation properties in the time-dependent Hartree Fock theory, Phys Rev C. 77 (2008), 041301, https://doi.org/10.1103/PhysRevC.77.041301 (R).
[8] G. Scamps, D. Lacroix, Effect of pairing on one- and two-nucleon transfer below the Coulomb barrier: a time-dependent microscopic description, Phys Rev C. 87 (2013), 014605, https://doi.org/10.1103/PhysRevC.87.014605.
[9] P. Goddard, S. Paul, A. Rios, Fission dynamics within time-dependent Hartree-Fock: deformation-induced fission, Phys Rev C. 92 (2015), 054610, https://doi.org/10.1103/PhysRevC.92.054610.
[10] J. Alexander Maruhn, P.-G. Reinhard, S. Paul, S.A. Umar, The TDHF code Sky3D, Comput Phys Commun. 185 (2014) 2195, https://doi.org/10.1016/j.cpc.2014.04.008.
[11] P.A.M. Dirac, Note on exchange phenomena in the thomas atom, Proc Camb Phil Soc. 26 (1930) 376–385, https://doi.org/10.1017/S0305004100016108.
[12] S.A. Umar, V.E. Oberacker, Three-dimensional unrestricted time-dependent Hartree-Fock fusion calculations using the full Skyrme interaction, Phys Rev C. 73 (2006), 054607, https://doi.org/10.1103/PhysRevC.73.054607.
[13] K. Washiyama, D. Lacroix, Energy dependence of the nucleus-nucleus potential close to the Coulomb barrier, Phys Rev C. 78 (2008), 024610, https://doi.org/10.1103/PhysRevC.78.024610.
[14] D.J. Kedziora, C. Simenel, New inverse quasifission mechanism to produce neutron-rich transfermium nuclei, Phys Rev C. 81 (2010), 044613, https://doi.org/10.1103/PhysRevC.81.044613.
[15] E. Chabanat, B. Paul, P. Haensel, J. Meyer, R. Schaeffer, A Skyrme parameterization from subnuclear to neutron star densities Part II. Nuclei far from stabilities, Nucl Phys. 635 (1998) 231–256, https://doi.org/10.1016/S0375-9474(98)00180-8.
[16] M. Bender, P.-H. Heenen, P.-. Reinhard, Self-consistent mean-field models for nuclear structure, Rev Mod Phys. 75 (2003) 121–180, https://doi.org/10.1103/RevModPhys.75.121.
[17] P. Klüpfel, P.-G. Reinhard, T.J. Bürvenich, J.A. Maruhn, Variations on a theme by Skyrme: a systematic study of adjustments of model parameters, Phys Rev C. 79 (2009), 034310, https://doi.org/10.1103/PhysRevC.79.034310.
[18] S. Goriely, S. Hilaire, A.K., M. Sin, R. Capote, Towards a prediction of fission cross sections on the basis of microscopic nuclear inputs, Phys Rev C. 79 (2009), 024612, https://doi.org/10.1103/PhysRevC.79.024612.
[19] M. Kortelainen, T. Lesinski, J. Moŕe, W. Nazarewicz, J. Sarich, Nicolas Schunck, M.V. Stoitsov, S. Wild, Nuclear energy density optimization, Phys Rev C. 82 (2010), 024313, https://doi.org/10.1103/PhysRevC.82.024313.
[20] Y. Hashimoto, K. Nodeki, A numerical method of solving time-dependent Hartree-Fock-Bogoliubov equation with Gogny interaction, 2007, https://doi.org/10.48550/arXiv.0707.3083. (accessed July 20, 2007).
[21] C. Simenel, S.A. Umar, Heavy-ions collisions and fission dynamics with the time-dependent Hartree-Fock theory and its extensions, Prog Part Nucl Phys. 103 (2018) 19–66, https://doi.org/10.1016/j.ppnp.2018.07.002.
[22] B. Paul, S. Elliot Koonin, J.W. Negele, One-dimensional nuclear dynamics in the time-dependent Hartree-Fock approximation, Phys Rev C. 13 (1976) 1226–1258, https://doi.org/10.1103/PhysRevC.13.1226.
[23] M. Ghafouri, H. Sadeghi, M. Torkiha, Self-consistent description of the SHFB equations for 112Sn, Results Phys. 8 (2018) 734–743, https://doi.org/10.1016/j.rinp.2017.12.076.
[24] M. Engel, D.M. Brink, K. Goeke, S.J. Krieger, D. Vautherin, Time-dependent Hartree-Fock theory with Skyrme's interaction, Nucl Phys. 249 (1975) 215–238, https://doi.org/10.1016/0375-9474(75)90184-0.

[25] F. Villars, D.J. Rowe, Dynamic structure of nuclear states, Oxford University Press, London, 1972.
[26] S. Elliot Koonin, Hydrodynamic approximations to time-dependent Hartree-Fock, Massachusetts Institute of Technology, (Ph.D. thesis), 1975.
[27] R. Graetzer, J.X. Saladin, Quadrupole moments of 2^+ states of even tin isotopes, Phys Rev C. 12 (1975) 1462–1468, https://doi.org/10.1103/PhysRevC.12.1462.
[28] G.F. Bertsch, P. Francesco Bortignon, R.A. Broglia, Damping of nuclear excitations, Rev Mod Phys. 55 (1983) 287–314, https://doi.org/10.1103/RevModPhys.55.287.